ACS OMEGA

Open Access

http://pubs.acs.org/journal/acsodf

Article

Preparation of Self-Healing Anthocyanidin-Containing Thermochromic Alginate Ink for Authentication Purposes

Amal T. Mogharbel, Gadeer R. S. Ashour, Kholood Alkhamis, Ameena M. Al-bonayan, Matokah M. Abualnaja, Jihan Qurban, Hanadi A. Katouah, and Nashwa M. El-Metwaly*

Cite This: *ACS Omega* 2024, 9, 1562−1572

Read Online

ACCESS | Metrics & More | Article Recommendations

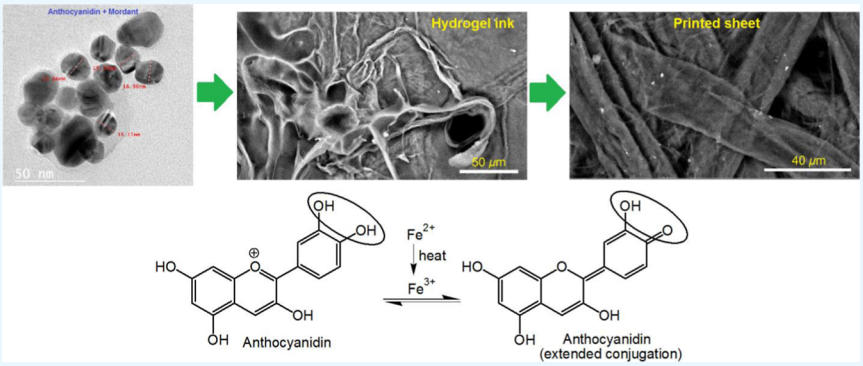

ABSTRACT: Thermochromic inks have proven to be a promising security encoding approach for making commercially available products less susceptible to forgery. However, thermochromic inks have been plagued with poor durability. Thus, self-healable hydrogels can be used as self-repair inks with better durability. Herein, we combined hybrid cellulose nanofibers (CNFs) and sodium alginate (SA) with anthocyanidin(Cy)-based *Brassica oleracea* L. var. *capitata* extract in the existence of mordant (ferrous sulfate) to create a self-healing ink for authentication. CNFs were used as a reinforcement agent to enhance the mechanical strength of the sodium alginate hydrogel. Both durability and thermal stability were ensured using self-healing inks. Red cabbage was used to extract Cy-based chromophore as an environmentally friendly spectroscopic probe for immobilization into SA. Using varying concentrations of anthocyanidin, self-healable composite hydrogels (Cy@SA) with thermochromic properties were provided. Using the CIE Lab color coordinate system, homogeneous purple (569 nm) films were printed onto a sheet surface. Upon heating from 25 to 70 °C, the purple color changed to red (433 nm). Transmission electron microscopy was applied to study anthocyanidin/mordant (Cy/M) nanoparticles (NPs). The properties of the applied prints were analyzed using several methods. Both the hydrogel and stamped sheets were tested for their mechanical and rheological characteristics, respectively. Research on the nanocomposite ink (Cy@SA) antibacterial properties and cytotoxicity was also conducted.

1. INTRODUCTION

The forgery of government papers, banknotes, and commercial objects has had catastrophic security and economic effects across the globe. The counterfeiting industry has been monitored to contribute billions to the black market. Therefore, there is an urgent need for research into advanced anticounterfeiting technology and materials.[1−3] According to previous reports, optical features are effective anticounterfeiting security measures due to being easy to check but challenging to imitate. Quantum dots have been described as potential optical authentication materials in recent years. Their outstanding emission efficiency and small and evenly sized particles Bode well for their potential usage in anticounterfeiting applications.[4] However, because of their reliance on very short emissions, anticounterfeiting materials are vulnerable to fluorescence interference with the printed medium. Authentication of official documents including passports, banknotes, certificates, and identification cards has grown more important in recent years. Consequently, a plethora of authentication methods have been described.[5] Newer forms of identification methods include quick response (QR) encoding, holographic labeling, and radio frequency identification (RFID) card.[6−8] However, such anticounterfeiting designs come at significant cost and complicated procedures. Fabricating innovative materials with

Received: October 13, 2023
Revised: November 27, 2023
Accepted: November 30, 2023
Published: December 15, 2023

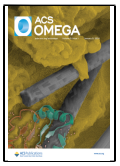

thermochromic characteristics is therefore crucial to the development of cutting-edge authentication devices free of background interferences.[9] Recently, anticounterfeiting ink made from a variety of thermochromic materials such as polymer dots and supramolecular hydrogels, has been reported.[10,11] Thermochromism is a temperature-triggered reversible phase transition between two different color states of different wavelengths. The development of temperature-induced chromic polymer ink has been the focus of recent studies because of their remarkable stability and colorimetric qualities.[12] Owing to their poor reflectance and high surface area, thermochromic nanoparticles of polymer ink can display remarkable optical qualities. However, the problem arises when these polymer nanoparticles cluster together and cause printer nozzles to get blocked.[13] Thus, the use of thermochromic nanoparticles distributed in a polymer matrix is an advanced method for more reliable identification.

Functional materials are distinguished with native features and functions.[14,15] They can be reported as a category of engineered structures with suitable surface morphology.[16−18] In particular, a colorimetric thermometer is intriguing as it provides a straightforward tool for monitoring of temperature by the observation of colorimetric variations without the need for specialized equipment or trained staff.[19] Paints, thermometer strips, inks, switchers, sensors, mapping probes, and smart windows are some of the numerous commercial and scientific applications of thermochromic pigments.[20−22] Due to their fast responsiveness, a nanoparticle polymer thermometer composed of nanostructured self-assemblies is of special interest. Thermometers based on polymers are often made using a number of different polymers and chromophores.[23] Hydrogel-based colorimetric thermometers are gaining popularity as a means of mapping cellular temperatures *in vivo*. As thermochromic agents, polymeric hosts and synthetic probes like boron-dipyrromethene and tricyanofuran-hydrazone have been used in aqueous environments.[24,25] However, such synthetic chromophores are unsafe for human consumption since they are nonbiodegradable and nonbiocompatible.[26] Anthocyanin pigments can be found in different plants and foods, such as red cabbage, raspberries, blueberries, and black soybeans. They are natural flavonoid indicators that are classified under the phenolic category.[27−29] Their appearance in water changes according to the pH value, displaying red in very acid surroundings, greenish yellow in moderately alkaline media, pink in moderately acid solutions, colorless in strongly basic media, and purple at neutral pH.[30] Anthocyanins are safe for human ingestion since they are found naturally in numerous plants and are utilized as a food coloring agent. The anticancer and antioxidant characteristics of anthocyanins due to their quenching capability toward reactive oxygen species have also been explored.[31] Intriguing studies have been conducted on the creation of self-healing anti-counterfeiting materials. However, conventional anticounterfeiting methods have limitations, such as poor durability.[32] Self-healable materials can repair themselves after being damaged, thereby prolonging their service life.[33,34] For this reason, advanced anticounterfeiting applications have placed a premium on the preparation of self-healing secure inks.[35,36] Sodium alginate (SA) has been described as a naturally occurring self-healing carbohydrate polymer characterized with biodegradability, nontoxicity and biocompatibility. Many pharmaceutical compounds, including skin care items, have found suitable and friendly matrixes in SA-based self-healing hydrogels. SA has been used in food industries as emulsifier, stabilizer, thickening agent, and gelling agent.[37,38] It has been typically used in its hydrogel form in many fields such as drug delivery, tissue engineering, biomedicine, and wound dressing.[39−41] Therefore, SA can be used as a useful composite hydrogel merged with an anthocyanidin (Cy)-based red-cabbage extract using ferrous sulfate as a mordant agent.

To the best of our knowledge, a self-healable anthocyanidin-containing anticounterfeiting hydrogel has not been presented yet. Herein, we prepared a color-tunable hydrogel by dissolving varying concentrations of anthocyanin extract in the self-healing CNFs-reinforced sodium alginate hydrogel in the presence of mordant (ferrous sulfate). Authentication stamps made from manufactured thermochromic Cy@SA ink can be applied to various products such as currency and certified documents. The thermochromic properties of the nanocomposite hydrogels changed depending on the anthocyanin concentration. The hydrogel layer imprinted on the paper surface appeared purple (569 nm) under ambient conditions but became red (433 nm) upon heating from 25 to 70 °C. The stamped film prevents erasure and scratches and cannot be substituted with other counterfeit inks, making it ideal for use on paper documents. Direct dyes such as anthocyanidin are said to be very water-soluble. Therefore, ferrous sulfate mordant is used in the printing of anthocyanin on the paper surface. Both the nontoxic natural material anthocyanidin biomolecule and sodium alginate biomacromolecule can be described as environmentally friendly materials. To create a thermochromic nanocomposite ink, anthocyanidin/mordant nanoparticles (Cy/M NPs) were admixed with sodium alginate. Thermochromic phenomenon was seen in the heated stamped films, making this a viable method for providing anticounterfeiting secure designs with a temperature-stimulated colorimetric shift. The present strategy can be applied as a reliable ink by several sectors to combat counterfeiting.

2. EXPERIMENTAL SECTION

2.1. Materials. Hydrochloric acid (ACS Reagent; 37%) and ferrous sulfate ($FeSO_4$) were obtained from Merck (Egypt). Sodium alginate [$M = 6.4 \times 10^4$ g/mol; M/G = 0.46 for M (β-D-mannuronic acid) units and 0.54 for G (α-L-guluronic acid) units] was supplied from Sigma-Aldrich (Egypt). For printing thermochromic designs, we sourced some off-white, circular-chapped Whatman paper from Aldrich (Egypt) with 240 mm diameter, 87 g m^{-2} weight, 180 μm thickness, and 11 μm pore size. Wood pulp (bleached) was kindly supplied from Qina Co. for Paper Production (Egypt). Sodium bromide, methanol, hydrochloric acid, sodium hydroxide (NaOH), (2,2,6,6-tetramethylpiperidin-1-yl)oxidanyl (TEMPO), and sodium hypochlorite were obtained from Sigma-Aldrich (Egypt). Cellulose nanofibers were prepared according to a modified method published earlier.[39] Red cabbage was purchased from a local market (Egypt). Anthocyanins can be easily extracted from cabbage due to their low cost, high availability, and fast-growing rate. Anthocyanidin was isolated from red cabbage using a modified version of the previously described method.[27]

2.2. Preparation of Cellulose Nanofibers. Wood pulp (2 g) in distilled water was combined with TEMPO (0.34 g) and NaBr (0.34 g). The provided mixture was stirred for 30 min to guarantee the formation of a uniform dispersion. Under ambient conditions, an aqueous medium of sodium hypochlorite was added slowly to the above-mentioned mixture. The pH of the produced solution was brought to 10 by the addition of sodium hydroxide (0.5 M). An excessive quantity of absolute ethanol

https://doi.org/10.1021/acsomega.3c07874
ACS Omega 2024, 9, 1562−1572

was then added to stop the oxidation progress. After repeated filtrations at a pH value of 7, the produced cellulose nanofibers were freeze-dried.

2.3. Extraction of Anthocyanidin. *Brassica oleracea* L. var. *capitata* (600 g) was finely chopped and macerated in an admixture of methyl alcohol and distilled water (1:3; 300 mL). Then, the aforementioned solution was acidified to a pH of 2 using hydrochloric acid diluted in water (1 mol L^{-1}). The mixture was kept for 3 days in the fridge at 4 °C. The filtered mixture was centrifuged at a rate of 2000 rpm for 15 min. The remaining reddish solution was extracted using chloroform after the solid remnants were removed. A rotary evaporator set to 40 °C was used to expose the solvent to evaporation. The given solution became a dark reddish violet after being treated with strong hydrochloric acid in a refluxing bath. A dark brown powder (anthocyanidin chloride) was obtained by chilling the solution after extraction. The resulting powder was then desiccated after being sifted. Methanol was utilized as an eluent in the purification of the extract using Sephadex LH-20. The provided anthocyanide (1.5 mg) was dissolved in methanol (5 mL) to produce a standardized solution of anthocyanidin. The provided mixture was stabilized after being chilled for an hour. HPLC Agilent 1100 (Waldborn, Germany) was used to analyze the extracted anthocyanin solution. By adding a tiny amount of magnesium strip and hydrochloric acid (1 mL), Shinoda's experiment[33] was able to determine the anthocyanidin flavonoid character.

2.4. Preparation of Hydrogels. A colorless aqueous solution of sodium alginate (1 g) in distilled water (10 mL) was prepared by heating for an hour at 85 °C. Another homogeneous aqueous suspension of cellulose nanofibers (0.4 wt %) in distilled water was prepared by homogenization (ultrasonic treatment) at 25 kHz for 30 min. The aforementioned suspension of cellulose nanofibers was combined with the provided sodium alginate aqueous solution at a ratio of 10:90, respectively.[39] The admixture was subjected to stirring for 30 min and ultrasonicated (25 kHz) for 15 min to guarantee the creation of a homogeneous, transparent, and viscous solution. Different amounts of anthocyanidin were added to CNFs/SA. For 15 min, the resulting solutions were admixed by mechanical stirring. Cy@SA was mixed with 5% ferrous sulfate. After being swirled for 60 min and exposed to ultrasonic (25 kHz) for 15 min, the given mixture was well mixed. Each ratio of anthocyanidin, including 0, 0.5, 1, 2, 3, 4, 5, 6, and 7% (w/w), was denoted by a separate set of symbols, including Cy_0, Cy_1, Cy_2, Cy_3, Cy_4, Cy_5, Cy_6, Cy_8, and Cy_8, respectively. The hydrogel inks that were created had a purple and sticky appearance. Wooden stamps were then used to imprint the hydrogels onto a Whatman paper. After applying the designs, we let them dry for 20 min in the air. Drop casting of the above solutions also yielded purple films of Cy@SA, which were air-dried in a Petri dish (Teflon) for 60 min. Both of the casted films and stamped sheets were placed in a dry box until analysis could be performed.

2.5. Analysis and Characterization. *2.5.1. Morphological Studies.* The morphology of Cy/M particles was studied by a JEOL 1230 (JEOL, Japan) at an accelerating voltage of 80 kV after they were dispersed in distilled water and subjected to sonication (25 kHz) for 30 min. Nexus 670 (Thermo Nicolet, Madison, WI, USA) was utilized to determine infrared spectra (FTIR) of stamped sheets in the range of 4000−400 cm^{-1} at a resolution of 2.0 cm^{-1} and averaging 64 scans. The morphology and structural composition of Cy@SA casted films and prints were analyzed using a scanning electron microscopy (SEM) Quanta FEG 250 (Czech) connected with energy dispersive X-ray spectroscopy (EDX; TEAM model) at an acceleration voltage of 30 kV and a working distance of 21 mm.

2.5.2. Rheological Study. Using a Brookfield model DV-III (Stoughton, MA) with Brookfield software, we were able to ascertain the hydrogel ink (Cy_5) rheological characteristics. According to the previously reported procedure,[21] the rheometer was first leveled and autozeroed. Viscosities of the hydrogels were reported at different concentrations of anthocyanidin. The sample (8 mL) was charged into a removable chamber connected to a temperature probe with an accuracy of 0.1 °C.

2.5.3. Mechanical Properties. The mechanical behavior of prints in the form of rectangles (15 mm × 140 mm) was reported using Zwick universal equipment (Zwick, Ulm, Germany). According to the previously reported procedure,[23] the wire length between crossheads was adjusted at 5 mm, and the load was adjusted at 2000 N with a crosshead speed of 10 mm/min.

2.5.4. Thermochromic Properties. To investigate the thermochromic behavior of the dry hydrogel film printed on a paper sheet at a neutral pH value (7.0) in an aqueous solution (5%; w/v), the absorption spectra were recorded when the temperature was altered between 25 and 70 °C. To test the reversibility of the thermometer, the temperature range was systematically pushed between 25 and 70 °C. After each heating−cooling cycle, the absorption spectra were recorded. The cloud points of the Cy@SA hydrogels were determined by heating at a rate of 5 °C min^{-1} in a water bath.[35,36] When the first sign of turbidity appeared, the temperature was noted as the cloud point.

2.5.5. Coloration Measurements. We analyzed color strength (K/S), absorbance spectra, and CIE Lab parameters (L^*, a^*, and b^*) of the dry-printed paper sheets using HunterLab Ultrascan Pro (United States). Ultrascan Pro was utilized to rapidly report the coloration changes after the printed paper was heated to the desired temperature. The colorimetric parameters were expressed by L^* representing brightness from white (100) to black (0), a^* representing color between reddish ($+a^*$) and greenish ($-a^*$), and b^* representing color between yellowish ($+b^*$) and bluish ($-b^*$).[42] CIE is abbreviated for *French* name (Commission Internationale de Eclairage) of the International Commission on Illumination. Canon A710IS was utilized to take photographic images of Cy_5.

2.5.6. Biological Properties. Under MTT [3-(4,5-dimethylthiazol-2-yl)-2,5-diphenyltetrazolium bromide; Sigma-Aldrich, Egypt] proliferation assay, the cytotoxicity (*in vitro*) test of the Cy@SA hydrogel was established using human (normal) epithelial cell lines (BJ1). A stock solution of MTT in a phosphate-buffered saline (12 mM) was charged into each well. The cytotoxic activity (%) was calculated by eq 1.[43]

$$\text{Cytotoxicity (\%)} = \left(\frac{\text{Reading of sample}}{\text{Reading of negative control}} - 1\right) \times 100 \quad (1)$$

The Cy@SA hydrogel films were examined for their capability to inhibit the growth of *Escherichia coli* and *Staphylococcus aureus* using conventional plate agar counting procedures. The bacterial reduction (R %) was determined by eq 2.[44]

$$\text{Bacterial reduction } (R\ \%) = \frac{(A - B)}{A} \times 100 \quad (2)$$

https://doi.org/10.1021/acsomega.3c07874
ACS Omega 2024, 9, 1562−1572

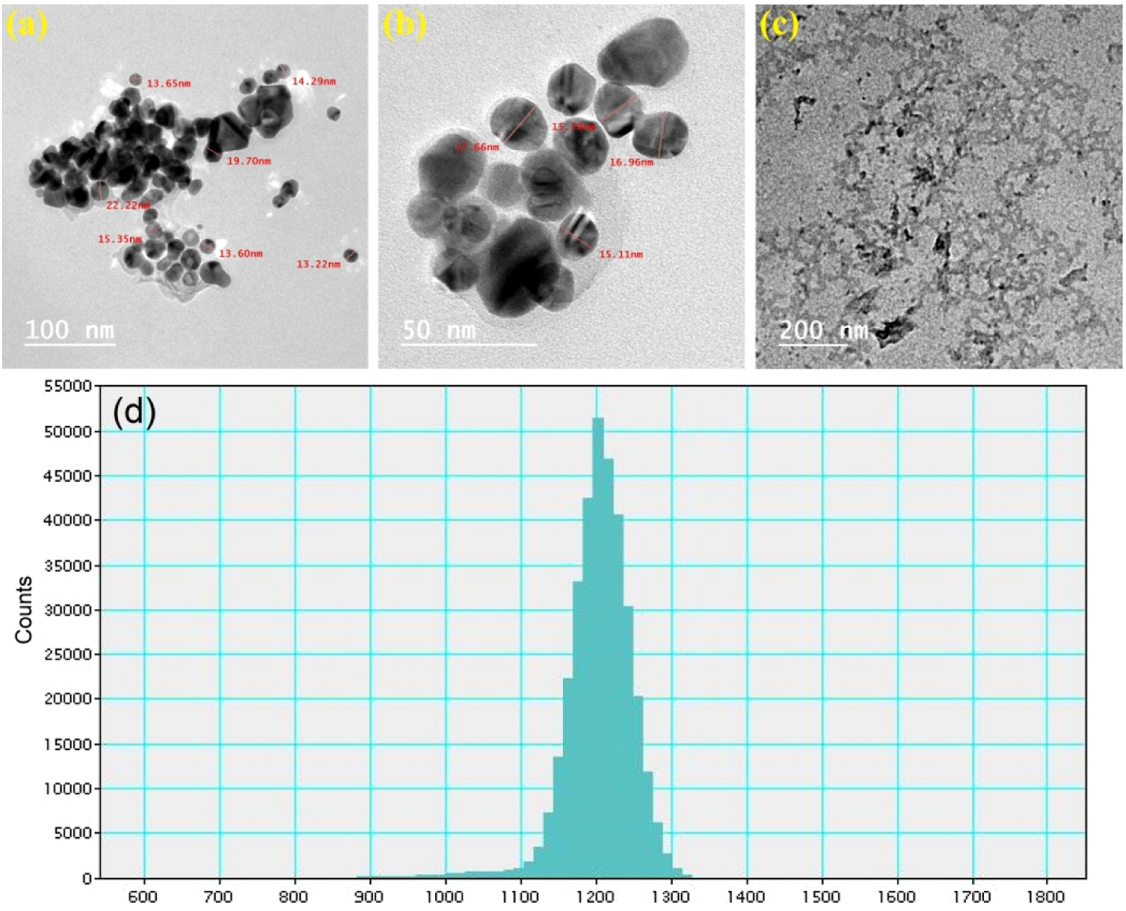

Figure 1. TEM analysis of Cy/M NPs (a,b), CNFs (c), and histogram view for the mean particle value of Cy/M (d).

where *A* is the bacterial colony count of the blank specimen and *B* is the bacterial colony count of thermochromic specimen.

3. RESULTS AND DISCUSSION

3.1. Preparation of Thermochromic Hydrogel. Because anthocyanin is classified as a direct dye with high water-solubility, ferrous sulfate was used as a mordant to permanently embed the anthocyanidin into the cellulose paper. After homogenizing (25 kHz) anthocyanidin and ferrous sulfate in distilled water for 30 min, we obtained Cy/M NPs for TEM analysis. NPs of Cy/M were found to have diameters of 12−22 nm as shown in Figure 1a,b. A histogram view of the mean particle value of Cy/M is shown in Figure 1d. Anthocyanidin was isolated from red cabbage using HCl and methanol. The UV−vis absorbance spectra were used to identify the flavonoid and phenolic compounds found in red cabbage extract to indicate three absorption maxima in the range of 283, 331, and 538 nm.[27−31]

Cellulose nanofibers were employed as a reinforcement nanofiller in the sodium alginate biocomposite to improve the mechanical performance of the prepared hydrogel. CNFs were prepared from bleached wood pulp employing a mixture of NaBr/TEMPO/NaClO.[39] TEM analysis of CNFs demonstrated widths in the range of 29−57 nm (Figure 1c). Aqueous solutions of CNFs and SA were admixed to provide transparent and viscous composite hydrogels. The above-mentioned solution was utilized to prepare smart inks with different concentrations of anthocyanidin. A wooden stamp was employed as an authenticating pattern to imprint the Cy@SA hydrogels onto the paper surface. The incorporation of anthocyanidin into a matrix of CNFs/SA led to the formation of a photochromic ink. CNFs were used to reinforce the mechanical performance of SA hydrogel, and to prevent clumping of Cy/M NPs.[39] Thus, no hydrogel was produced in the absence of CNFs. Additionally, the presence of flavonoids in the anthocyanin extract was confirmed using Shinoda's technique[31] by adding a little amount of Mg strip and a small amount of HCl to produce a reddish solution. Table 1 summarizes the HPLC analysis of anthocyanin, which shows

Table 1. HPLC Analysis of *B. oleracea* L. var. *capitata* Extract

phenol	quantity (wt %)
acacetin	0.75
gallic acid	0.82
kaempferol	46.05
ferulic acid	18.02
vanillin	0.84
quercetin-7-methyl ether	0.70
chlorogenic acid	2.09
p-coumaric acid	2.07
chrysin	0.95
quercetin	3.10
catechin	0.62
quercetin-7,3′-dimethyl ether	4.25
cinnamic acid	1.28
rutin	19.62
caffeic acid	0.83

https://doi.org/10.1021/acsomega.3c07874
ACS Omega 2024, 9, 1562−1572

the presence of bioactive phenols. The maximum absorbance of Cy@SA stamped paper shifts from purple (569 nm) to red (433 nm) when the temperature rises from 25 to 70 °C. The chemical switching mechanism linked with electron delocalization begins with deprotonation of anthocyanidin as the temperature rises. This deprotonation/protonation process can be reversed by altering the temperature of the system between 25 and 70 °C. Raising the temperature allows for the detection of four different isomers of anthocyanidin (Figure 2), including quinoid anion, carbinol anion, flavylium cation, and chalcone.[27,30] The flavylium cation (red) is the main isomeric form at elevated temperatures, whereas the flavylium ion (purple) dominates at lower temperatures.

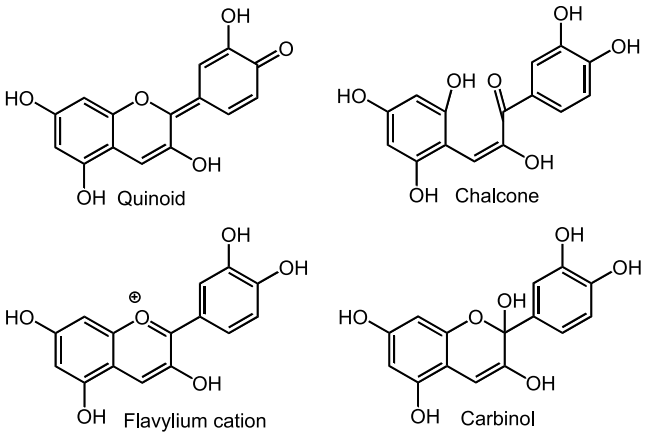

Figure 2. Different isomers of anthocyanidin.

Thick hydrogels were produced by adding varying quantities of anthocyanidin to an aqueous medium of sodium alginate. The solution of Cy@SA was then mordanted with ferrous sulfate. The hydrogel-based inks, once produced, had a purple hue. The paper was imprinted using ink made from hydrogels. The stamped film that exhibits temperature-induced chromism displayed anticounterfeiting security that turned from purple to red when heating from 25 to 70 °C.

3.2. Morphological Properties. Figure 3 displays an SEM micrograph showing that the surface of anthocyanidin-embedded cast sodium alginate film is almost like that of a pigment-free hydrogel film. Cy@SA design was printed onto sheets. Figure 4 depicts a morphological analysis of the thermochromic Cy@SA prints on the paper surface. Cy/M NPs were incorporated onto the sheet surface as illustrated by SEM micrographs. As shown in Figure 4, increasing the anthocyanidin content in the sodium alginate hydrogel had no discernible effect on the printed paper samples. The uniform distribution of Cy/M NPs on the surface of paper can also be explained by the formation of ferric coordination bonding with the cellulose hydroxyl oxygen. It has been stated that immobilization of nanoparticles makes uniform distribution onto different surfaces simpler than it is a dense material.[45] SEM ImageJ software showed that Cy/M NPs had diameters between 12 and 22 nm, which made it simpler to achieve uniform dispersion across the paper surface. Table 2 summarizes the results of the EDX examination of blank and printed paper samples. Carbon and oxygen were shown to be the primary elements of blank paper using EDX analysis. Iron was present in low concentration owing to the use of $FeSO_4$ as a mordant and was also confirmed by EDX analysis of prints, along with the presence of oxygen and carbon, the two primary elements of the cellulose sheet and the anthocyanidin chromophore. The elemental concentrations of Cy_0, Cy_1, Cy_5, and Cy_8 as determined by EDX were almost the same across three scanned

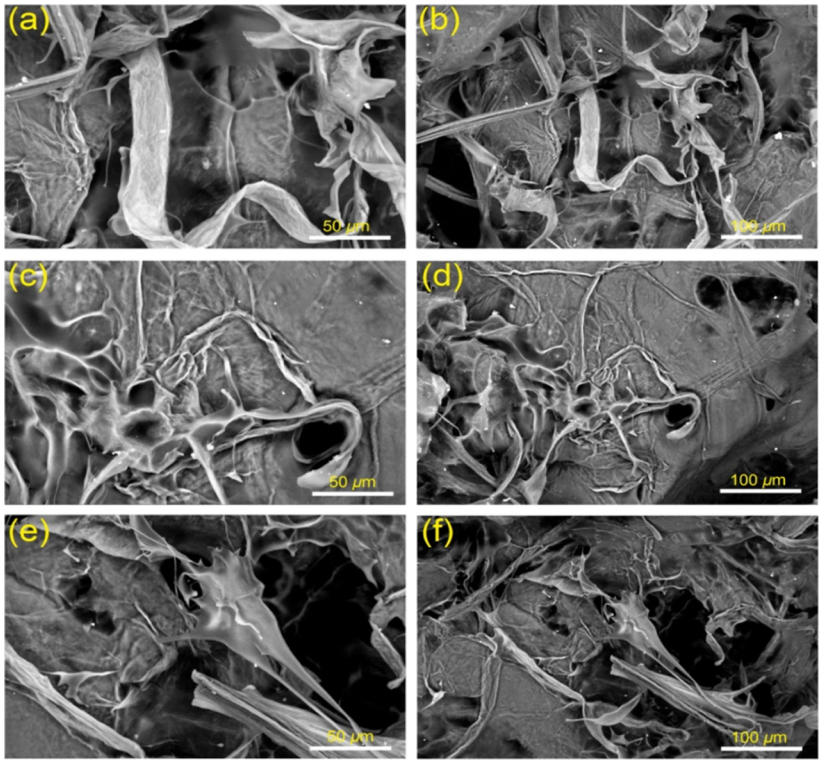

Figure 3. SEM analysis of drop-casted dry hydrogel films from Cy@SA; Cy_1 (a,b), Cy_5 (c,d), and Cy_8 (e,f).

https://doi.org/10.1021/acsomega.3c07874
ACS Omega 2024, 9, 1562−1572

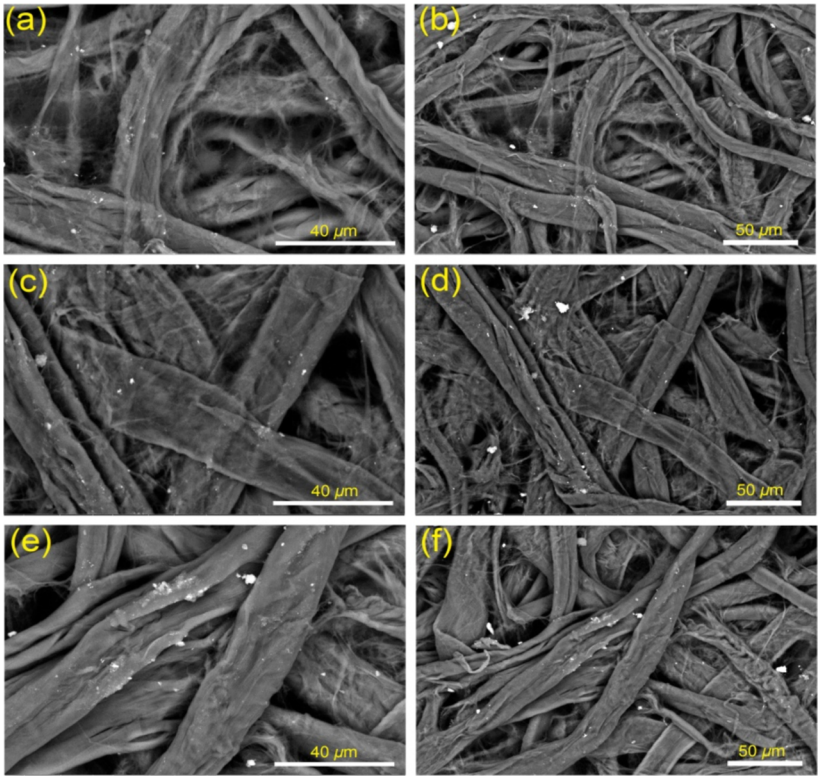

Figure 4. SEM analysis of paper sheets printed with Cy@SA; Cy_1 (a,b), Cy_5 (c,d), and Cy_8 (e,f).

Table 2. EDX Analysis (wt %) of Cy_0, Cy_1, Cy_5, and Cy_8 at Different Sites (St_1, St_2, and St_3) on Paper Surface

print		C	O	Fe
Cy_0		66.54	33.46	0
Cy_1	St_1	65.96	33.59	0.45
	St_2	65.63	33.82	0.55
	St_3	65.86	33.53	0.61
Cy_5	St_1	65.42	33.55	1.03
	St_2	65.66	33.34	1.00
	St_3	65.42	33.51	1.07
Cy_8	St_1	65.58	32.76	1.66
	St_2	64.49	33.76	1.75
	St_3	64.72	33.64	1.64

places on the paper surface, demonstrating a uniform distribution of Cy/M over the sheet surface. The elemental compositions matched the elemental ratios used to make the Cy@SA thermochromic prints, as shown by the EDX analysis.

Absorbance peaks at 3405 cm^{-1} from the paper cellulose hydroxyl stretching vibration, 2985 cm^{-1} from the C−H aliphatic stretching vibration, and 1088 cm^{-1} from the aliphatic C−H bending vibration were detected in the infrared spectra of stamped papers (Figure 5). Another absorption band was observed at 1754 cm^{-1} due to the alginate carbonyl stretching vibration. After stamping, the Cy@SA coating was formed on the sheet surface, resulting in a reduction in the hydroxyl group intensity (3405 cm^{-1}). When more Cy/M was added to the sodium alginate medium, the intensity of the bands corresponding to the aliphatic C−H stretching and bending vibrations (2985 and 1088 cm^{-1}) also dropped. At the highest concentration of anthocyanidin, an apparent shift to a lower wavenumber value was observed for the alginate carbonyl stretching peak of Cy_8. This could be attributed to iron

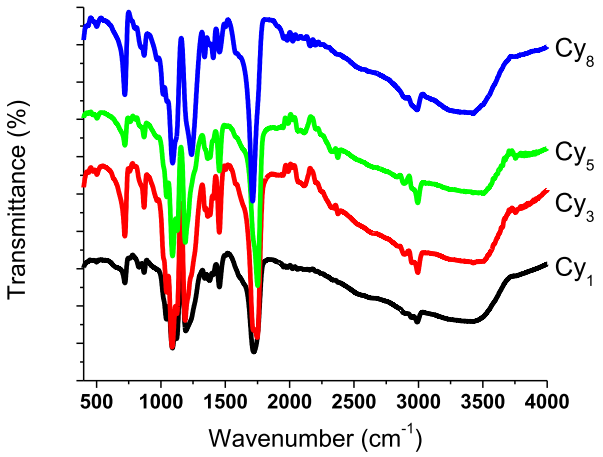

Figure 5. FTIR spectroscopic analysis of the Cy@SA prints.

coordination with the alginate carbonyl group and the anthocyanidin hydroxyl group.[28,30]

The gelation activity of Cy_5 was confirmed using the stable-to-inversion technique[46] as shown in Figure 6a,b. The self-healing property of the Cy@SA films can boost their resistance to mechanical damage, hence extending the hydrogel inks shelf life. As shown in Figure 6c, a circle able of bearing a mass of 100 g was created by self-healing of two-half circles (Cy_5) with 95% relative humidity when placed in contact with each other. Hydrogen bonds formed between the carboxylic carbonyl O atoms (H-bonding acceptor) and the hydroxyl H atoms (H-bonding donor) are responsible for the self-healing behavior.[35,36] Because it encourages the flow of H-bonding acceptor and donor to generate H-bonds across the damaged interface, humidity is crucial to improving the self-healing performance.

https://doi.org/10.1021/acsomega.3c07874
ACS Omega 2024, 9, 1562−1572

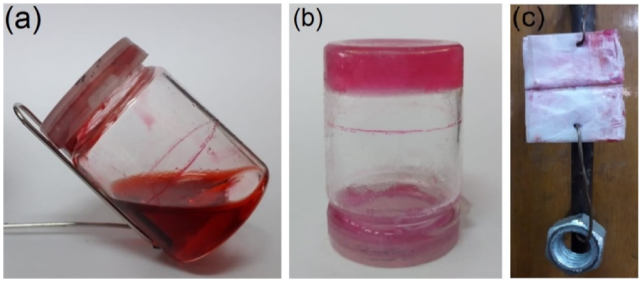

Figure 6. Photographs of hot (a) and cold (b) hydrogel (Cy_5) demonstrating the stable-to-inversion technique, and (c) self-healed two-half circles of hydrogel (Cy_1) able to withstand a mass of 100 g.

3.3. Rheology and Mechanical Assessments. Figure 7a displays the results of an investigation into the rheology of the Cy@SA hydrogel (Cy_5). Since the Cy@SA hydrogel flow rate was most closely matched by non-Newton's laws, the hydrogel exhibited comparatively high viscosity. The rate of shear was shown to linearly decrease the viscosity. The effect of a constant shearing rate (5 s^{-1}) on hydrogels of different anthocyanidin ratios is illustrated in Figure 7b. It was shown that the viscosity increases when the anthocyanidin ratio.

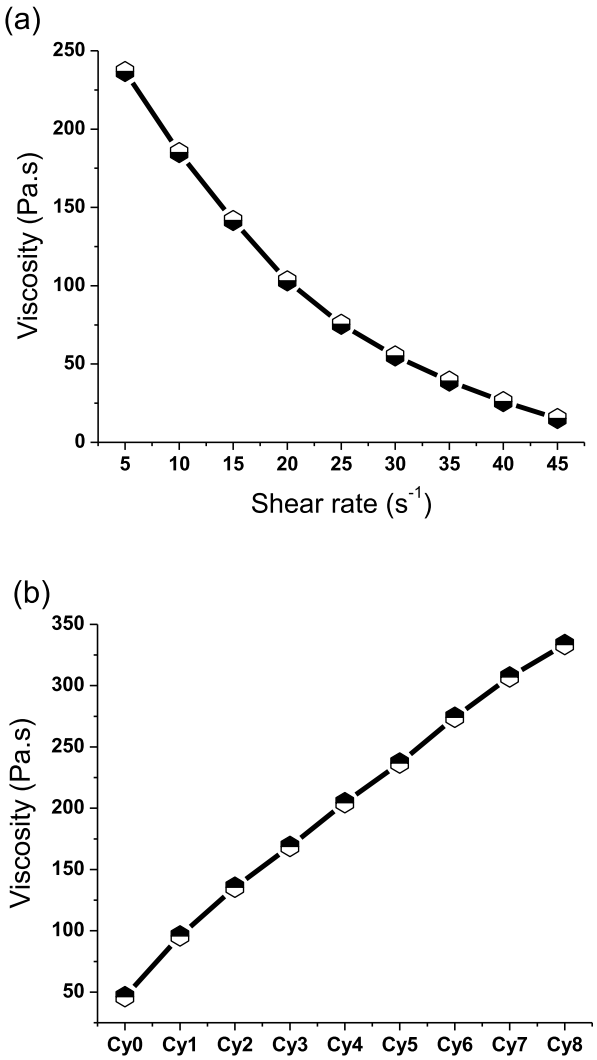

Figure 7. (a) Effect of different shearing rates on the viscosity of Cy_5 and (b) effect of constant shearing rate (5 s^{-1}) on hydrogels of different anthocyanidin ratios.

Tensile (TS) and Young's modulus (YM) of Cy_1 were observed to decline near strain % in comparison to Cy_0 due to YM being TS/strain dependent. Sodium alginate, a primary component of the hydrogel, displayed elasticity and adhesion, proving an increase in strain percent. Figure 8 displays that when the anthocyanidin concentration increased from Cy_1 to Cy_6, both YM and TS rose, and then remained constant as the ratio increased from Cy_6 to Cy_8. This could be attributed to the coagulation of Cy/M NPs, increasing the gaps between cellulose microfibers. Minor shifts in strain % were seen with increasing anthocyanidin concentration, which can be attributable to the interfacial bonding formed between positive charges on Cy/M NPs and negative charges on the cellulose surface. Therefore, the cross-linking process between cellulosic fibers is enhanced by the incorporation of Cy/M particles into the paper surface. The Cy/M NPs are kept on the paper surface by the sodium alginate hosting bulk, either by coordinative bonding between the negative charges on the cellulosic sheet and the positively charged Cy/M NPs or through physical trapping of the anthocyanidin in the sodium alginate bulk.

3.4. Colorimetric Properties. The colorimetric changes of Cy@SA prints were analyzed by CIE Lab as demonstrated in Table 3. The printed patterns undergo an instantaneous purple-to-red color shift when heated from 25 to 70 °C as shown in Figure 9. However, the printed patterns took ∼55 min to recover their original purple color upon cooling to 25 °C. Changing the anthocyanidin ratio from Cy_1 to Cy_5 resulted in minor shifts in CIE Lab and K/S values. Thermochromism from purple to red was confirmed by a rise in L^* upon increasing the temperature from 25 to 70 °C. The $+a^*$ values were stable from 25 to 70 °C, but the $-b^*$ values flipped to become positive. A purple hue is established by the $+a^*$ and $-b^*$ values, whereas a red hue is produced by the $+a^*$ and $+b^*$ values. K/S rose with higher anthocyanidin ratios, indicating a deeper purple color. In addition, a rise in K/S at higher temperatures denoted a transition in colorimetry from purple to red of high tinctorial strength. Upon increasing the temperature from 25 to 70 °C, slight changes were detected in both color strength and CIE Lab parameters of samples from Cy_5 to Cy_8. Thus, the optimum thermochromic efficiency was reported for Cy@SA with a 4% anthocyanidin to anthocyanidin ratio (Cy_5).

The absorption spectra of Cy_5 upon heating from 25 to 70 °C are shown in Figure 10. The absorbance intensity at 433 nm was found to rise linearly with temperature, whereas the absorbance intensity at 569 nm decreased. A purplish coordination complex (Cy/M) was formed between iron(III) and hydroxyl groups in both cellulose and anthocyanidin.[47,48] As the temperature increases, the extent of coordination deteriorates. When the temperature increased, several other hues were apparent. Figure 11 shows how this modifies the strength of the thermochromic effect.

As shown in Figure 12, several heating and cooling cycles were performed on a Cy@SA print to assess its thermal stability. As the temperature rose, purple Cy_5 was seen to become red. Multiple heating/cooling cycles showed no change in absorption intensity, proving the material thermal stability.

3.5. Biological Properties. After 24 h, cell viability in Cy_5 was 97%, as reported by the MTT experiment.[43,49] After 48 h, 94% of the cells were still alive, demonstrating great cytocompatibility (Table 4). A slight decrease in cell viability was detected upon increasing the anthocyanidin concentration.

https://doi.org/10.1021/acsomega.3c07874
ACS Omega 2024, 9, 1562−1572

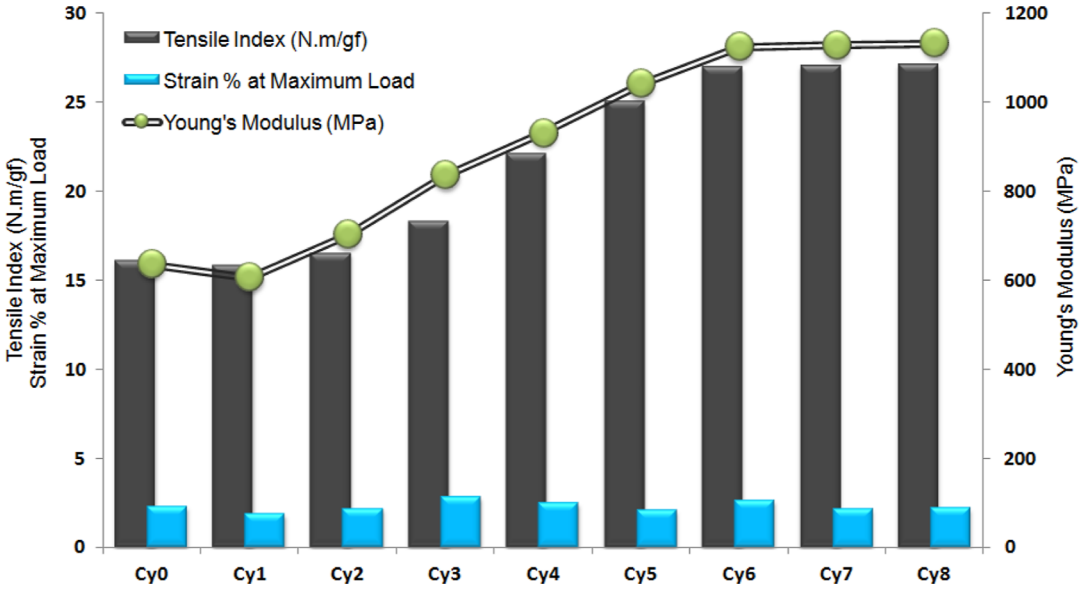

Figure 8. Impacts of the anthocyanidin ratio on the mechanical behavior of Cy@SA prints.

Table 3. Colorimetric Behavior of Cy@SA Prints at 25 and 70 °C[a]

anthocyanidin	color strength		L^*		a^*		b^*	
	25 °C	70 °C	25 °C	70 °C	25 °C	70 °C	25 °C	70 °C
Cy_0	0.41	0.65	92.56	92.67	0.10	0.03	−1.26	1.03
Cy_1	1.31	3.09	58.48	63.36	21.02	7.37	−5.25	3.51
Cy_2	1.47	3.18	56.47	62.55	19.42	8.08	−7.51	3.11
Cy_3	1.75	3.76	54.07	61.64	17.44	10.2	−8.68	2.86
Cy_4	1.89	4.21	53.60	58.63	13.72	13.42	−10.66	2.67
Cy_5	1.92	4.45	50.29	56.73	12.97	16.3	−12.99	2.40
Cy_6	2.22	4.58	48.13	55.82	10.46	20.62	−15.09	2.04
Cy_7	2.31	4.87	47.01	55.18	9.76	24.22	−16.14	1.88
Cy_8	2.58	5.13	46.31	54.68	9.24	25.54	−16.74	1.52

[a]The lightness shift from black (0) to white (100) is denoted by L^*, the color changes between red (+) and green (−) are symbolized by a^*, and the coloration changes between yellowish (+) and bluish (−) are symbolized by b^*.

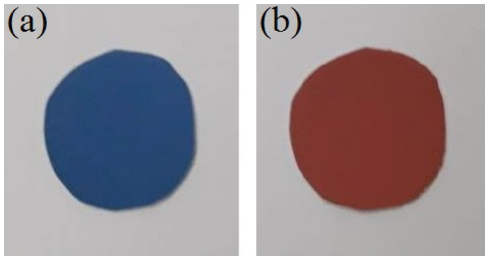

Figure 9. Effect of temperature on the stamped film of Cy_5, displaying a purple (a) to red (b) color shift upon heating from 25 to 70 °C, respectively.

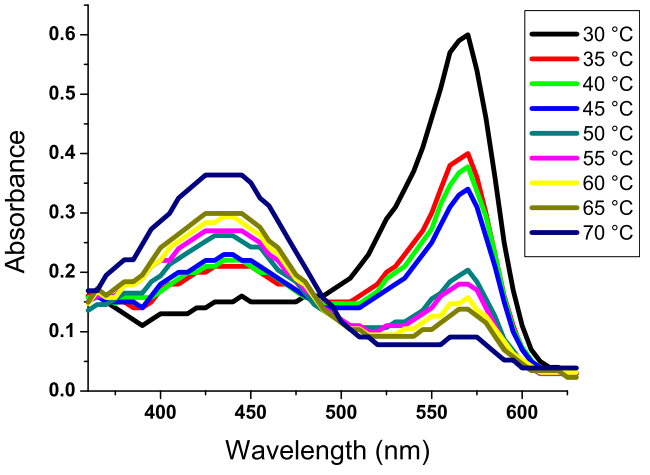

Figure 10. Effect of temperature on absorption spectra of Cy_5.

The growth inhibition of *E. coli* and *S. aureus* by the casted Cy@SA films is shown in Table 4. The blank film (Cy_0) could not kill germs since it does not include any antibacterial agents. Bacteria could not survive on the cast Cy@SA film with the lowest anthocyanidin concentration (Cy_1). The ratio of anthocyanidins rose, and the reduction of bacteria improved.

4. CONCLUSIONS

New self-healing thermochromic hydrogel inks were prepared and printed onto sheets of paper, changing their color from purplish (569 nm) to reddish (433 nm) upon raising the temperature from 25 to 70 °C. We used absorbance spectra, color strength, and CIE Lab characteristics to analyze the color shifts in the printed materials. High thermal stability and endurance were shown by an anthocyanidin chromophore extracted from red cabbage and used as a spectroscopic sensor in the creation of nanocomposite hydrogels using ferrous sulfate

https://doi.org/10.1021/acsomega.3c07874
ACS Omega 2024, 9, 1562−1572

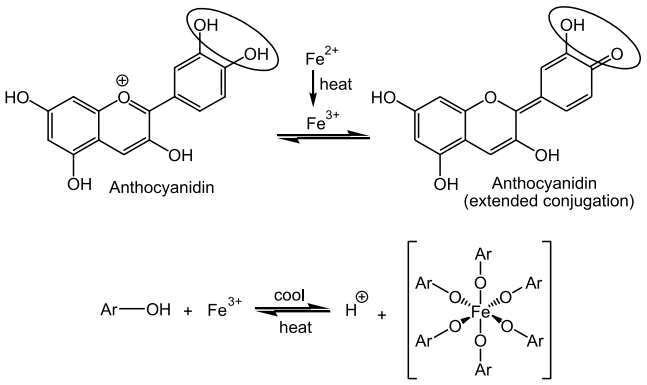

Figure 11. Proposed mechanism for the creation/dissociation of Cy/M complex; Ar is the anthocyanidin hydroxyl functional substituent.

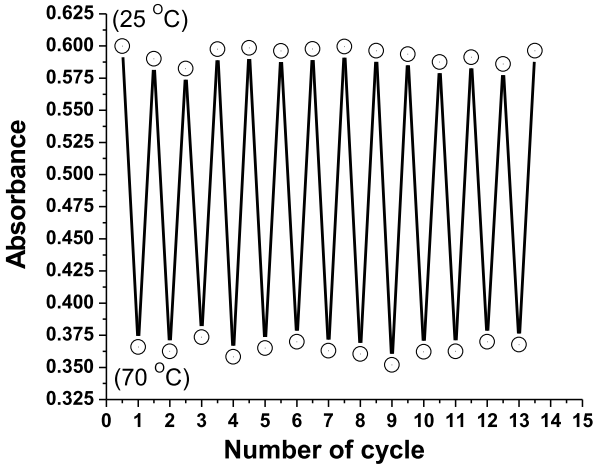

Figure 12. Intensity of absorption band (Cy_5) at 433 nm under heating (70 °C) and cooling (25 °C) cycles to prove thermal stability.

Table 4. Cell Viability of Casted Cy@SA Films after 24 and 48 h, and Their Antibacterial Activities against *E. coli* and *S. aureus*

film	cell viability (%)		reduction of bacteria (%)	
	24 h	48 h	*S. aureus*	*E. coli*
Cy_1	99 ± 1.2	97 ± 1.0	29 ± 1.3	34 ± 1.1
Cy_2	99 ± 1.6	95 ± 1.2	33 ± 1.7	37 ± 1.1
Cy_3	98 ± 1.4	95 ± 1.5	36 ± 1.0	41 ± 1.3
Cy_4	97 ± 1.4	95 ± 1.0	42 ± 1.1	46 ± 1.0
Cy_5	97 ± 1.3	94 ± 1.1	47 ± 1.3	51 ± 1.1
Cy_6	96 ± 1.0	93 ± 1.1	50 ± 1.5	54 ± 1.2
Cy_7	95 ± 1.0	93 ± 1.5	51 ± 1.1	59 ± 1.4
Cy_8	95 ± 1.1	92 ± 1.2	52 ± 1.6	61 ± 1.2

mordant. To make a composite ink, a mixture of anthocyanidin (thermochromic agent), cellulose nanofibers (reinforcement agent), sodium alginate (self-healing agent), and ferrous sulfate (mordant) was used. The highest thermochromic efficiency was reported for Cy@SA with a 4% anthocyanidin ratio. Cy/M NPs were 12−22 nm in diameter, whereas the widths of the cellulose nanofibers ranged from 29 to 57 nm. Without causing any cytotoxicity, Cy@SA displays temperature-dependent color changes. The current thermochromic ink can be utilized in a variety of products owing to its self-healing properties, low cost, being environmentally friendly, and efficient anticounterfeiting applications. The existing thermometer might be used to create intelligent clothing with built-in temperature monitoring capabilities. It can be used as a temperature indication sticker to place on bottles of hot syrup.

■ ASSOCIATED CONTENT

Data Availability Statement

All data generated or analyzed during this study are included in this published article.

■ AUTHOR INFORMATION

Corresponding Author

Nashwa M. El-Metwaly − *Department of Chemistry, Faculty of Applied Science, Umm-Al-Qura University, 24382 Makkah, Saudi Arabia; Department of Chemistry, Faculty of Science, Mansoura University, 35516 Mansoura, Egypt;* orcid.org/0000-0002-0619-6206; Email: nmmohamed@uqu.edu.sa, n_elmetwaly00@yahoo.com

Authors

Amal T. Mogharbel − *Department of Chemistry, College of Science, University of Tabuk, 71474 Tabuk, Saudi Arabia*

Gadeer R. S. Ashour − *Department of Chemistry, Faculty of Applied Science, Umm-Al-Qura University, 24382 Makkah, Saudi Arabia*

Kholood Alkhamis − *Department of Chemistry, College of Science, University of Tabuk, 71474 Tabuk, Saudi Arabia*

Ameena M. Al-bonayan − *Department of Chemistry, Faculty of Applied Science, Umm-Al-Qura University, 24382 Makkah, Saudi Arabia*

Matokah M. Abualnaja − *Department of Chemistry, Faculty of Applied Science, Umm-Al-Qura University, 24382 Makkah, Saudi Arabia*

Jihan Qurban − *Department of Chemistry, Faculty of Applied Science, Umm-Al-Qura University, 24382 Makkah, Saudi Arabia*

Hanadi A. Katouah − *Department of Chemistry, Faculty of Applied Science, Umm-Al-Qura University, 24382 Makkah, Saudi Arabia*

Complete contact information is available at: https://pubs.acs.org/10.1021/acsomega.3c07874

Notes

The authors declare no competing financial interest.

Ethical Approval: Not applicable.

Consent to Publish: The author(s) agree to publish the article under the Creative Commons Attribution License.

■ REFERENCES

(1) Ren, W.; Lin, G.; Clarke, C.; Zhou, J.; Jin, D. Optical nanomaterials and enabling technologies for high-security-level anticounterfeiting. *Adv. Mater.* **2020**, *32*, 1901430.

(2) Hong, W.; Yuan, Z.; Chen, X. Structural color materials for optical anticounterfeiting. *Small* **2020**, *16*, 1907626.

(3) Abdollahi, A.; Roghani-Mamaqani, H.; Razavi, B.; Salami-Kalajahi, M. Photoluminescent and chromic nanomaterials for anticounterfeiting technologies: Recent advances and future challenges. *ACS Nano* **2020**, *14*, 14417−14492.

(4) Du, K.; Zhang, M.; Li, Y.; Li, H.; Liu, K.; Li, C.; Feng, J.; Zhang, H. Embellishment of upconversion nanoparticles with ultrasmall perovskite quantum dots for full-color tunable, dual-modal luminescence anticounterfeiting. *Adv. Opt. Mater.* **2021**, *9*, 2100814.

(5) Deng, J.; Deng, L.; Guan, Z.; Tao, J.; Li, G.; Li, Z.; Li, Z.; Yu, S.; Zheng, G. Multiplexed anticounterfeiting meta-image displays with single-sized nanostructures. *Nano Lett.* **2020**, *20*, 1830−1838.

(6) Zhou, H.; Han, J.; Cuan, J.; Zhou, Y. Responsive luminescent MOF materials for advanced anticounterfeiting. *Chem. Eng. J.* **2022**, *431*, 134170.
(7) Li, Z.; Liu, X.; Wang, G.; Li, B.; Chen, H.; Li, H.; Zhao, Y. Photoresponsive supramolecular coordination polyelectrolyte as smart anticounterfeiting inks. *Nat. Commun.* **2021**, *12*, 1363.
(8) Li, Z.; Wang, G.; Ye, Y.; Li, B.; Li, H.; Chen, B. Loading photochromic molecules into a luminescent metal-organic framework for information anticounterfeiting. *Angew. Chem.* **2019**, *131*, 18193−18199.
(9) Crosby, P. H. N.; Netravali, A. N. Green Thermochromic Materials: A Brief Review. *Adv. Sustainable Syst.* **2022**, *6*, 2200208.
(10) Liu, Y.; Zheng, C.; Yang, B. Phosphorus and Nitrogen Codoped Carbonized Polymer Dots with Multicolor Room Temperature Phosphorescence for Anticounterfeiting Painting. *Langmuir* **2022**, *38*, 8304−8311.
(11) Hu, Y.-P.; Naeem, M.; Wang, J.; Yao, H.; Zhang, Y.-M.; Wei, T.-B.; Lin, Q. Aggregation Induced Emission Supramolecular Functionalized Benzimidazole Hydrogel for Metal-Ion Responsive and Fluorescent Anti-Counterfeiting,. *ChemistrySelect* **2022**, *7*, No. e202202348.
(12) Alidaei-Sharif, H.; Roghani-Mamaqani, H.; Babazadeh-Mamaqani, M.; Sahandi-Zangabad, K.; Abdollahi, A.; Salami-Kalajahi, M. Photochromic polymer nanoparticles as highly efficient anti-counterfeiting nanoinks for development of photo-switchable encoded tags. *J. Photochem. Photobiol., A* **2023**, *436*, 114343.
(13) Liu, Y.; Chen, W.; Lu, L.; Yang, B. Si-assisted N, P Co-doped room temperature phosphorescent carbonized polymer Dots: Information Encryption, graphic Anti-counterfeiting and biological imaging. *J. Colloid Interface Sci.* **2022**, *609*, 279−288.
(14) Liu, W.; Huang, F.; Liao, Y.; Zhang, J.; Ren, G.; Zhuang, Z.; Zhen, J.; Lin, Z.; Wang, C. Treatment of CrVI-containing Mg (OH) 2 nanowaste. *Angew. Chem.* **2008**, *120*, 5701−5704.
(15) He, M. Y.; Ren, T. X.; Jin, Z. D.; Deng, L.; Liu, H. J.; Cheng, Y. Y.; Li, Z. Y.; Liu, X. X.; Yang, Y.; Chang, H. Precise analysis of potassium isotopic composition in plant materials by multi-collector inductively coupled plasma mass spectrometry. *Spectrochim. Acta, Part B* **2023**, *209*, 106781.
(16) Li, M.; Xia, Q.; Lv, S.; Tong, J.; Wang, Z.; Nie, Q.; Yang, J. Enhanced CO 2 capture for photosynthetic lycopene production in engineered Rhodopseudomonas palustris, a purple nonsulfur bacterium. *Green Chem.* **2022**, *24*, 7500−7518.
(17) Ahmad, H. A.; Ahmad, S.; Gao, L.; Ismail, S.; Wang, Z.; El-Baz, A.; Ni, S. Q. Multi-omics analysis revealed the selective enrichment of partial denitrifying bacteria for the stable coupling of partial-denitrification and anammox process under the influence of low strength magnetic field. *Water Res.* **2023**, *245*, 120619.
(18) Zhao, Y.; Dong, Y.; Chen, X.; Wang, Z.; Cui, Z.; Ni, S. Q. Using sulfide as nitrite oxidizing bacteria inhibitor for the successful coupling of partial nitrification-anammox and sulfur autotrophic denitrification in one reactor. *Chem. Eng. J.* **2023**, *475*, 146286.
(19) Lee, J.; Yang, H.; Park, C. H.; Cho, H.-H.; Yun, H.; Kim, B. J. Colorimetric thermometer from graphene oxide platform integrated with red, green, and blue emitting, responsive block copolymers. *Chem. Mater.* **2016**, *28*, 3446−3453.
(20) Kumar, K.; Stefanczyk, O.; Chorazy, S.; Nakabayashi, K.; Ohkoshi, S.-I. Ratiometric and Colorimetric Optical Thermometers Using Emissive Dimeric and Trimeric {[Au (SCN) 2]-} n Moieties Generated in d-f Heterometallic Assemblies. *Angew. Chem.* **2022**, *134*, No. e202201265.
(21) Snari, R. M.; Al-Qahtani, S. D.; Aldawsari, A. M.; Alnoman, R. B.; Ibarhiam, S. F.; Alaysuy, O.; Shaaban, F.; El-Metwaly, N. M. Development of novel reversible thermometer from N-isopropylacrylamide and dicyanodihydrofuran hydrazone probe. *Polym. Eng. Sci.* **2022**, *62*, 3820−3830.
(22) Cui, Y.; Zou, W.; Song, R.; Yu, J.; Zhang, W.; Yang, Y.; Qian, G. A ratiometric and colorimetric luminescent thermometer over a wide temperature range based on a lanthanide coordination polymer. *Chem. Commun.* **2014**, *50*, 719−721.
(23) Al-Ahmed, Z. A.; Snari, R. M.; Alsoliemy, A.; Katouah, H. A.; Bayazeed, A.; Abumelha, H. M.; El-Metwaly, N. M. Preparation of thermochromic and vapochromic cotton fibers finished with poly (N-vinylcaprolactam-co-hydrazone). *Cellulose* **2022**, *29*, 8457−8472.
(24) Dang, H.; Tian, Y.; Cheng, Q.; Teng, C.; Xie, K.; Yan, L. Galactose conjugated boron dipyrromethene and hydrogen bonding promoted J-aggregates for efficiently targeted NIR-II fluorescence assistant photothermal therapy. *J. Colloid Interface Sci.* **2022**, *612*, 287−297.
(25) Elsawy, H.; Sedky, A.; Abou Taleb, M. F.; El-Newehy, M. H. Preparation of novel reversible thermochromic polyethylenimine dendrimer and tricyanofuran hydrazone chromophore. *Eur. Polym. J.* **2022**, *174*, 111344.
(26) Gürses, A.; Açıkyıldız, M.; Güneş, K.; Sadi Gürses, M.; Gürses, A.; Açıkyıldız, M.; Güneş, K.; Sadi Gürses, M. Classification of dye and pigments. In *Dyes and Pigments*; Springer, 2016; pp 31−45.
(27) Al-Qahtani, S. D.; Alzahrani, H. K.; Azher, O. A.; Owidah, Z. O.; Abualnaja, M.; Habeebullah, T. M.; El-Metwaly, N. M. Immobilization of anthocyanin-based red-cabbage extract onto cellulose fibers toward environmentally friendly biochromic diagnostic biosensor for recognition of urea. *J. Environ. Chem. Eng.* **2021**, *9*, 105493.
(28) Khattab, T. A.; El-Naggar, M. E.; Pannipara, M.; Wageh, S.; Abou Taleb, M. F.; Abu-Saied, M. A.; El Sayed, I. E. T. Green metallochromic cellulose dipstick for Fe (III) using chitosan nanoparticles and cyanidin-based natural anthocyanins red-cabbage extract. *Int. J. Biol. Macromol.* **2022**, *202*, 269−277.
(29) Roy, S.; Rhim, J.-W. Anthocyanin food colorant and its application in pH-responsive color change indicator films. *Crit. Rev. Food Sci. Nutr.* **2021**, *61*, 2297−2325.
(30) Nafady, A.; Al-Enizi, A. M.; Alothman, A. A.; Shaikh, S. F. Design and fabrication of green and sustainable vapochromic cellulose fibers embedded with natural anthocyanin for detection of toxic ammonia. *Talanta* **2021**, *230*, 122292.
(31) Alsahag, M.; Alisaac, A.; Al-Hazmi, G. A. A.; Pashameah, R. A.; Attar, R. M. S.; Saad, F. A.; El-Metwaly, N. M. Preparation of carboxymethyl cellulose/polyvinyl alcohol wound dressing composite immobilized with anthocyanin extract for colorimetric monitoring of wound healing and prevention of wound infection. *Int. J. Biol. Macromol.* **2023**, *224*, 233−242.
(32) Muthamma, K.; Sunil, D.; Shetty, P. Carbon dots as emerging luminophores in security inks for anti-counterfeit applications-An up-to-date review. *Appl. Mater. Today* **2021**, *23*, 101050.
(33) Liu, J.; Zhou, Y.; Lu, J.; Cai, R.; Zhao, T.; Chen, Y.; Zhang, M.; Lu, X.; Chen, Y. Injectable, tough and adhesive zwitterionic hydrogels for 3D-printed wearable strain sensors. *Chem. Eng. J.* **2023**, *475*, 146340.
(34) Wolfel, A.; Euti, E. M.; Picchio, M. L.; Romero, M. R.; Galván Josa, V. M.; Martinelli, M.; Minari, R. J.; Alvarez Igarzabal, C. I. Unraveling the gallol-driven assembly mechanism of thermoreversible supramolecular hydrogels inspired by ascidians. *Polym. Chem.* **2020**, *11* (45), 7185−7198.
(35) Alenazi, D. A. K.; AlSalem, H. S.; Alhawiti, A. S.; Binkadem, M. S.; Bukhari, A. A. H.; Alhadhrami, N. A.; Alatawi, R. A. S.; Abomuti, M. A. Development of strontium aluminate embedded photochromic cellulose hydrogel for mapping of fingermarks. *Inorg. Chem. Commun.* **2023**, *152*, 110669.
(36) Mogharbel, A. T.; Hameed, A.; Sayqal, A. A.; Katouah, H. A.; Al-Qahtani, S. D.; Saad, F. A.; El-Metwaly, N. M. Preparation of carbon dots-embedded fluorescent carboxymethyl cellulose hydrogel for anticounterfeiting applications. *Int. J. Biol. Macromol.* **2023**, *238*, 124028.
(37) Bahadoran, M.; Shamloo, A.; Nokoorani, Y. D. Development of a polyvinyl alcohol/sodium alginate hydrogel-based scaffold incorporating bFGF-encapsulated microspheres for accelerated wound healing. *Sci. Rep.* **2020**, *10*, 7342.
(38) Zhao, H.; Ouyang, X.-K.; Yang, L.-Y. Adsorption of lead ions from aqueous solutions by porous cellulose nanofiber-sodium alginate hydrogel beads. *J. Mol. Liq.* **2021**, *324*, 115122.

https://doi.org/10.1021/acsomega.3c07874
ACS Omega 2024, 9, 1562−1572

(39) Yue, Y.; Han, J.; Han, G.; French, A. D.; Qi, Y.; Wu, Q. Cellulose nanofibers reinforced sodium alginate-polyvinyl alcohol hydrogels: Core-shell structure formation and property characterization. *Carbohydr. Polym.* **2016**, *147*, 155−164.
(40) Zhu, Y.; Ma, Z.; Kong, L.; He, Y.; Chan, H. F.; Li, H. Modulation of macrophages by bioactive glass/sodium alginate hydrogel is crucial in skin regeneration enhancement. *Biomaterials* **2020**, *256*, 120216.
(41) Verma, A.; Thakur, S.; Mamba, G.; Gupta, R. K.; Gupta, R. K.; Thakur, P.; Thakur, V. K. Graphite modified sodium alginate hydrogel composite for efficient removal of malachite green dye. *Int. J. Biol. Macromol.* **2020**, *148*, 1130−1139.
(42) Abou-Melha, K. Preparation of photoluminescent nanocomposite ink toward dual-mode secure anti-counterfeiting stamps. *Arab. J. Chem.* **2022**, *15*, 103604.
(43) Awad, H. M.; Abd-Alla, H. I.; Mahmoud, K. H.; El-Toumy, S. A. In vitro anti-nitrosative, antioxidant, and cytotoxicity activities of plant flavonoids: a comparative study. *Med. Chem. Res.* **2014**, *23*, 3298−3307.
(44) Bhuyan, S.; Yadav, M.; Giri, S. J.; Begum, S.; Das, S.; Phukan, A.; Priyadarshani, P.; Sarkar, S.; Jayswal, A.; Kabyashree, K.; Kumar, A.; et al. Microliter spotting and micro-colony observation: A rapid and simple approach for counting bacterial colony forming units. *J. Microbiol. Methods* **2023**, *207*, 106707.
(45) Saravanan, A.; Kumar, P. S.; Karishma, S.; Vo, D.-V.; Jeevanantham, S.; Yaashikaa, P. R.; George, C. S. A review on biosynthesis of metal nanoparticles and its environmental applications. *Chemosphere* **2021**, *264*, 128580.
(46) Alsoliemy, A.; Alrefaei, A. F.; Almehmadi, S. J.; Almehmadi, S. J.; Hossan, A.; Khalifa, M. E.; El-Metwaly, N. M. Synthesis, characterization and self-assembly of new cholesteryl-substitued sym-tetrazine: Fluorescence, gelation and mesogenic properties. *J. Mol. Liq.* **2021**, *342*, 117543.
(47) Imani, H.; Gharanjig, K.; Ahmadi, Z. A novel efficient method for eco-friendly deep dyeing of wool yarns by extracted madder dyes in the presence of additives. *Ind. Crops Prod.* **2022**, *183*, 114970.
(48) El-Naggar, M. E.; Abu Ali, O. A.; Saleh, D. I.; Abu-Saied, M. A.; Khattab, T. A. Preparation of green and sustainable colorimetric cotton assay using natural anthocyanins for sweat sensing. *Int. J. Biol. Macromol.* **2021**, *190*, 894−903.
(49) Ahmed, E.; Maamoun, D.; Abdelrahman, M. S.; Hassan, T. M.; Khattab, T. A. Imparting cotton textiles glow-in-the-dark property along with other functional properties: photochromism, flame-retardant, water-repellency, and antimicrobial activity. *Cellulose* **2023**, *30*, 4041−4055.

https://doi.org/10.1021/acsomega.3c07874
ACS Omega 2024, 9, 1562−1572